NANOSHAVING OF BOVINE SERUM ALBUMIN FILMS ADSORBED ON MONOCRYSTALLINE SURFACES AND INTERFACES

Viliam KOLIVOŠKA[a1,*], Miroslav GÁL[a2], Štěpánka LACHMANOVÁ[a3,b], Pavel JANDA[a4], Romana SOKOLOVÁ[a5] and Magdaléna HROMADOVÁ[a6]

[a] *J. Heyrovský Institute of Physical Chemistry of Academy of Sciences of the Ccech Republic, v.v.i., Dolejškova 3, 182 23 Prague 8, Czech Republic; e-mail:* [1] *viliam.kolivoska@jh-inst.cas.cz,* [2] *miroslav.gal@jh-inst.cas.cz,* [3] *lachmanova@gmail.com,* [4] *pavel.janda@jh-inst.cas.cz,* [5] *romana.sokolova@jh-inst.cas.cz,* [6] *hromadom@jh-inst.cas.cz*

[b] *Department of Biochemistry, Faculty of Science, Charles University in Prague, Hlavova 2030, 128 40 Prague 2, Czech Republic*

Received April 19, 2011
Accepted May 11, 2011
Published online August 22, 2011

Paper submitted for a special issue of the Collection of Czechoslovak Chemical Communications devoted to "distinguished followers of the J. Heyrovský School of Polarography". This work is dedicated to Lubomír Pospíšil to commemorate his 70th birthday.

We apply the ex situ and in situ atomic force microscopy (AFM) nanoshaving technique to investigate the bovine serum albumin (BSA) films on Au(111) and highly oriented pyrolytic graphite (HOPG) surfaces. The both substrates were found to support the BSA films. The section analysis performed before and after the AFM nanoshaving allowed the determination of the film thickness. On Au(111) surface, both ex situ and in situ nanoshaving revealed that the film is formed by strongly denatured BSA molecules, with the average thickness 2.3 ± 0.2 and 2.0 ± 0.2 nm, respectively. On the other hand, the HOPG substrate was found to support less denatured BSA films, with the average film thickness 4.7 ± 0.3 and 5.2 ± 0.3 nm, based on the ex situ and in situ measurements, respectively.

Keywords: Proteins; Scanning probe microscopy; Surface analysis; Atomic force microscopy; Nanoshaving; Bovine serum albumin; Highly oriented pyrolytic graphite.

Besides being used in a high-resolution imaging[1,2] the scanning probe techniques may be exploited to transport material and form various nanostructures on surfaces and interfaces. These techniques are collectively called the scanning probe lithography (SPL). In the last decade, the SPL techniques attracted considerable attention due to their ability to form nano-patterned self-assembled monolayers (SAMs) and other nanostructures[3–6]. The SPL comprises atomic force microscopy (AFM) techniques such

doi:10.1135/cccc2011080

as nanoshaving[7], nanografting[8,9], dip-pen nanolitography[10] and local oxidation nanolitography[11] as well as scanning tunneling microscopy (STM) approaches, namely the electron induced diffusion[12] and desorption[13].

Nanoshaving is an AFM technique, in which a film formed on the surface or interface is intentionally displaced by the action of the AFM probe[3]. The film structure is first characterized by a (non-destructive) low force contact-mode AFM (CM AFM) or, alternatively, by employing a tapping mode AFM (TM AFM). Afterwards, a higher force is exerted in a selected area, causing the adsorbed material to be removed from its original position. The sample is then re-inspected by the low force CM AFM or by TM AFM[3]. When the supporting substrate withstands the applied forces, the depth of the nanoshaved area is equal to the film thickness. This allows the nanoshaving to be used as a quantitative surface analytical tool[14–20], both as an ex situ technique and in a liquid environment.

Nanografting[3–6,8,9] is very similar to the nanoshaving, but takes place in a solution of adsorbable species different from that being displaced by the AFM probe. The exposed substrate is subsequently refilled by the species from the solution, forming a two-component SAM with well-defined domains. As in nanoshaving, the formed nanostructures are investigated either by low force CM AFM or by TM AFM.

Nanoshaving and nanografting were applied to prepare and/or analyze various nanostructures. Xu et al.[8] nanografted the decanethiol ($C_{10}SH$) SAM in the presence of $C_{18}SH$ molecules, forming the nanoislands of $C_{18}SH$ surrounded by the $C_{10}SH$ SAM. In a related study[9], the authors nanografted the $C_{18}SH$ SAM in the solution of $HSC_{15}COOH$, forming hydrophilic islands in the hydrophobic matrix. Seo et al.[21] employed the combination of nanoshaving and electrodeposition to form the $C_{16}SH$ SAM nanografted by the silver nanoparticles. Staii et al.[22] nanografted the protein-resistant polyethyleneglycol-terminated SAM in the solutions of poly-D-lysine and laminin. The both polypeptides were found to adsorb on the exposed areas and the formed domains supported the growth of the neuronal cells. Rezek et al.[15] exploited both the ex situ and in situ nanoshaving to investigate the film assembled from the fetal bovine serum on the monocrystalline diamond surface. The diamond surface was further exploited in a related study[16], in which the nanoshaving was applied to determine the thickness of hybridized DNA arrays. Rosa et al.[14] measured the thickness of the film formed of 2-(4-pyridylethyl)trietoxysilane (PETS) on the oxidized silicon. The histogram constructed from the vertical differences induced by the nanoshaving showed two peaks. The authors concluded that the molecule of PETS may be cleaved at two different positions, which was also sup-

ported by theoretical calculations. Lee at al.[23] used in situ nanoshaving and subsequent re-imaging to write and read letters and lines into the octadecyldimethylmonochlorosilane SAM. The indented lines were further exploited as the sites for the self-assembly of the DNA molecules. Brower et al.[18] employed insitu nanoshaving to determine the thickness of the self-assembled multilayers of 4,4′-dimercaptobiphenyl formed by Cu(II) catalyzed oxidation on Au(111) surface. The values obtained for the monolayer, bilayer and trilayer were in a good agreement with those predicted theoretically.

Bovine serum albumin (BSA) is one of the most abundant proteins on the Earth. Its molecule forms a prolate spheroid with the dimensions 14 × 4 × 4 nm in the bulk of the solution[24]. The protein has numerous applications in biochemistry[25] and electrochemistry[26]. Recently, it was shown that it may be used as the nanobubble tracer on highly oriented pyrolytic graphite (HOPG) surface[27,28]. The AFM techniques showed that BSA molecules adsorb on various surfaces such as glass[29], mica[30,31], HOPG [32,33], silicon wafers[34], dipalmitoylphosphatidylglycerol Langmuir–Blodgett monolayers on water[35], silica[36] and polystyrene[31]. However, studies employing advanced AFM techniques, such as nanoshaving and nanografting, are very rare. Shi et al.[37] nanoshaved the BSA layer ex situ on polycrystalline borosilicate substrates. The substrate was subsequently immersed into the micellar solution of 1-palmitoyl-2-oleoyl-sn-glycero-3-phosphocholine (POPC). Fluorescence microscopy showed that the POPC molecules selectively adsorb on nanoshaved areas. Tencer et al.[38] employed the ex situ nanoshaving technique to study the BSA films on polycrystalline gold stripes. The average BSA film thickness (ca. 2 nm) was found to be considerably smaller than the dimensions of the BSA molecule in the bulk of aqueous solutions. The authors concluded that the film is formed by the denatured BSA molecules.

Herein, we employ both in situ and ex situ nanoshaving technique to investigate BSA films on two monocrystalline surfaces – Au(111) and HOPG. Monocrystalline surfaces offer significant advantages over polycrystalline ones, such as enhanced imaging resolution and increased reproducibility of the sample preparation. To the best of our knowledge, there is no study applying the AFM nanoshaving to investigate the BSA films on monocrystalline surfaces. Understanding the structure of the BSA films in situ is a prerequisite necessary for our future studies focusing on the interactions between BSA molecules or other biologically active molecules and air nanobubbles.

EXPERIMENTAL

Bovine serum albumin was purchased from Sigma–Aldrich (fraction V, >96%). Deionized water with a maximum resistivity of 18 MΩ cm was obtained by means of a Milli-Q RG purification system (Millipore Co., USA) and was used throughout the studies.

Water solutions of BSA were prepared by dissolving a respective amount of BSA in 2.0 ml of deionized water. The vessels intended for the solution preparation were cleaned by freshly prepared Piranha solution (concentrated sulfuric acid/concentrated hydrogen peroxide, 3:1 v/v), washed by deionized water and dried in the air.

Hydrogen-annealed mica-supported Au(111) surface was purchased from Agilent and used as received. Highly oriented pyrolytic graphite (HOPG, Structure Probe Inc., USA) was cleaved by the adhesive tape prior to use. The BSA films were obtained by the immersion of a substrate (either Au(111) or HOPG) to BSA solutions for two hours. The substrates were then washed by deionized water and dried in the stream of nitrogen. The BSA films on HOPG were prepared from solutions at six different concentrations: 50, 100, 200, 500, 1000 and 2000 ppm. The BSA films on Au(111) were prepared from the 1000 ppm solution.

All dried films were first scrutinized by ex situ AFM imaging and nanoshaving. Subsequently, the films formed from 1000 ppm solutions (on both Au(111) and HOPG) were immersed in deionized water and inspected in situ.

All AFM measurements were carried out on Agilent 5500 SPM (Agilent Technologies). The measurements employed the "Type II MAClevers" AFM probes with the nominal resonant frequency f_N = 75 kHz (reference range 45–115 kHz) and nominal force constant k_N = 2.8 N/m (reference range 0.5–9.5 N/m). The true force constant, k, of a cantilever was determined by measuring its resonant frequency, f, and employing the cubic interpolation in the k vs f dependence.

The images taken before and after the nanoshaving were all obtained in the TM AFM regime. Besides the topography information, the phase shift between the driving alternating voltage and the probe oscillation was recorded. It represents the complementary qualitative information about the structures on the interfaces.

The nanoshaving was performed in the constant force CM AFM mode, with a small repulsive force applied. Prior to each nanoshaving experiment, the force-distance spectroscopy experiment was performed in order to determine the exact loading force value. The deflection sensitivity of a given laser/cantilever configuration, S, defined as the ratio of the laser deflection, D, (measured in volts) and the cantilever deflection, z, (expressed in meters) was determined from the slope in the repulsive part of the laser deflection – distance (D vs z) curve. The obtained S value was employed to calculate the cantilever deflection Δz from the ΔD value. The latter quantity was kept constant with the aid of the feedback electronics. The applied repulsive force, F, was calculated employing the Hooke law, $F = -k\Delta z$. Typically, the force values were in the range of 20–40 nN, in both ex situ and in situ nanoshaving.

Both AFM imaging and nanoshaving was always performed with the same AFM probe, usually at the recording speed 0.5–2 line/s. All images were obtained at the resolution 512 pixels. The topography images shown in Results and discussion are all plane-corrected.

The values of the film thickness are presented in the form $\langle x \rangle \pm ts/(N-1)^{1/2}$, where $\langle x \rangle$ is the average value and s the standard deviation of N = 30 individual measurements with t = 2.313 (for N = 30). Presented values of the film thickness are rounded to one decimal place, which represents the accuracy limit of the employed AFM configuration.

The surface coverage is defined as the surface area occupied by a film divided by the total surface area i.e. the image-size squared. The occupied surface area was evaluated by counting the pixels with the *z* coordinate higher than a certain threshold that was kept constant throughout the analysis.

RESULTS AND DISCUSSION

Figure 1 shows characteristic ex situ TM AFM topography images of BSA films on HOPG.

The panels a, b and c show ex situ TM AFM topography images of the BSA films prepared from the BSA solutions with the concentration 50, 200 and 1000 ppm, respectively. The panel d shows the same area as in c after the CM AFM nanoshaving with the image-size 1 × 1 μm. The nanoshaving was also performed on the BSA films formed from solutions with other BSA concentrations. The corresponding images are not shown but resembled the one shown in the panel d. In all nanoshaving experiments carried out on the HOPG surface, the constant repulsive loading force of 25 nN was applied.

The nanoshaving procedure was intentionally carried out on an HOPG step (see panels c and d in Fig. 1). As can be seen, the HOPG step remains intact after the nanoshaving and therefore the procedure with the parame-

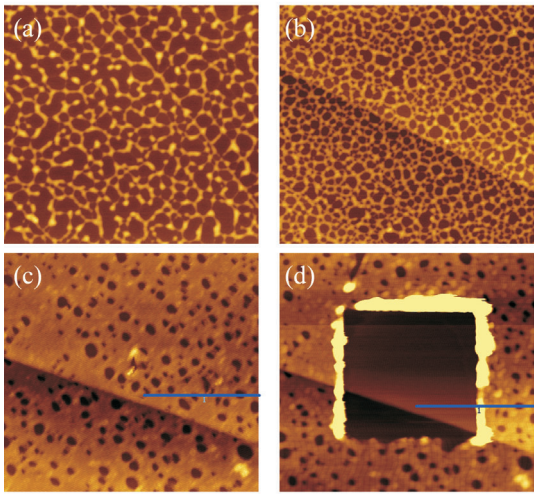

FIG. 1
BSA films on HOPG imaged by ex situ TM AFM, prepared from solutions with concentration 50 (a), 200 (b) and 1000 ppm (c). Panel d shows the same area as that in panel c after 1 × 1 μm nanoshaving. Image size 2 μm, height scale 15 nm

ters applied appears to be non-destructive to the underlying HOPG surface. For further confirmation of this presumption, the nanoshaving was accomplished on a pure surface of freshly cleaved HOPG with the repulsive forces up to 200 nN applied. The TM AFM images did not show any discernible topography changes. This confirms that the nanoshaving is non-destructive with respect to the underlying HOPG substrate and therefore the displaced material originates from the adsorbed BSA film.

The topography images obtained for the BSA films formed from solutions of all six concentrations were further scrutinized by the section analysis. Figure 2 shows the topography profiles obtained at solid blue lines shown in the panels c and d of Fig. 1. The two blue lines are located at the same location on the sample surface. Therefore, the topography changes caused by the nanoshaving procedure can be easily tracked.

The nanoshaving was carried out at locations corresponding to $x < 400$ nm in Fig. 2. The dashed green and the solid red line show the topography profile before and after the nanoshaving, respectively. The two profiles cross a hole at $x \sim 740$ nm. A positive topography structure centered at $x \sim 430$ nm corresponds to the accumulated material. As the underlying HOPG is not affected, the topography difference noticed for $x < 400$ nm is equal to the thickness of the BSA film (denoted by the arrow). The film thickness found by the nanoshaving procedure equals the depth of the hole located at

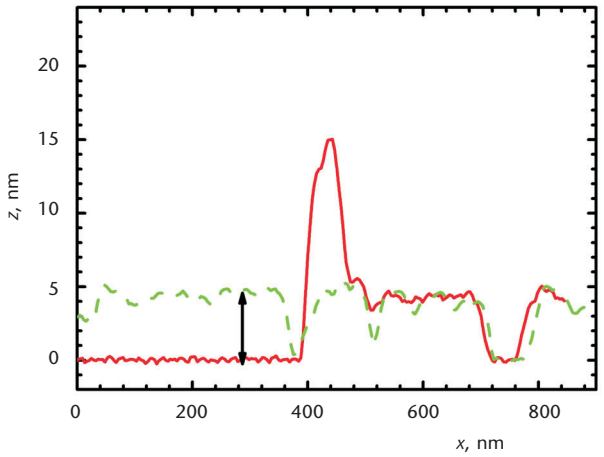

FIG. 2
Topography profiles obtained at solid blue lines in the panels c and d of Fig. 1. The dashed green line and the solid red line show the profile obtained before and after the nanoshaving, respectively. The black arrow denotes the film thickness

740 nm. This suggests that the bottom of the hole coincides with the HOPG surface. Figure 3a shows a histogram of the film thickness values obtained from thirty individual measurements of the height differences at various positions along the edges of the nanoshaved area. The histogram is constructed for the BSA film formed from the solution containing 1000 ppm of BSA. The same analysis was also applied to the films prepared at all other concentrations. Figure 3b shows a film thickness value as a function of the BSA concentration in the solution during the adsorption.

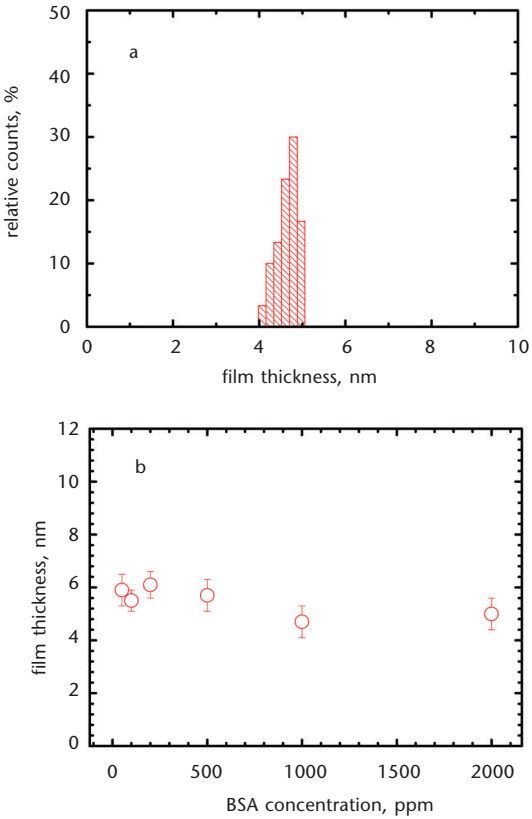

FIG. 3
Histogram of the film thickness values constructed for the ex situ BSA film formed from the 1000 ppm solution (a). The average ex situ film thickness as a function of the BSA concentration during the adsorption (b)

The film thickness is almost independent of the BSA concentration in the solution during the adsorption. On the other hand, the surface coverage was found to increase with the BSA concentration. Differences between the surface coverage of films formed from the solutions containing 50, 200 and 1000 ppm of BSA may be noticed in Fig. 1. Figure 4 shows the average surface coverage as a function of the BSA concentration during the adsorption. It was calculated from at least three 2 × 2 μm images obtained at different locations on the surface.

The films formed from the solutions containing 1000 and 2000 ppm repeatedly led to the films with the surface coverage approaching unity. However, the surface is never completely covered. The film always contains holes the depth of which is equal to the film thickness found by the nanoshaving procedure (see Fig. 2).

The presence of holes deserves a further discussion. When in contact with air-saturated water, HOPG surface is known to be covered with the nanobubbles[39], which were proved to influence the protein adsorption[27,28]. The surface portion occupied by the nanobubble cannot interact with the BSA molecules directly. Instead, the BSA molecules form ridges and rings around the nanobubbles. When taken out from the BSA solution, the nanobubbles cease to exist, leaving vacant sites in the BSA film formed on the HOPG surface[27,28].

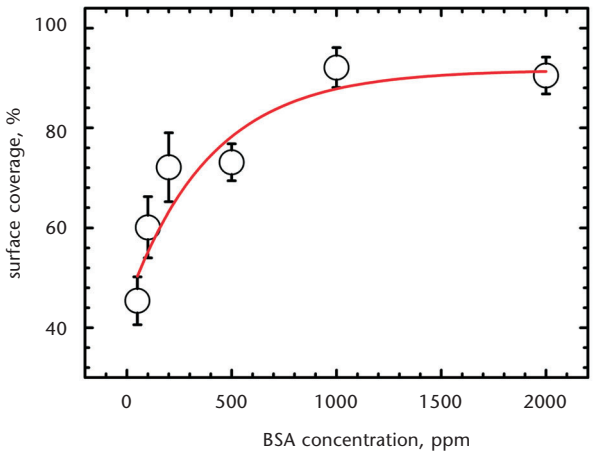

FIG. 4
Average surface coverage of ex situ BSA films as a function of the BSA concentration during the adsorption. Solid red line is shown just to guide the eye

The BSA film on HOPG formed from the 1000 ppm solution (panels c and d in Fig. 1) was immersed into pure water and scrutinized by in situ AFM imaging and nanoshaving techniques. Figure 5a shows the in situ 4 × 4 μm TM AFM topography image after the 2 × 2 μm CM AFM nanoshaving in the middle of the original image.

Figure 5b shows the profile measured at the position corresponding to the blue solid line in Fig. 5a. The dashed red lines in Fig. 5b denote the film thickness. The average film thickness, obtained from thirty measurements of topographic differences between the pristine and nanoshaved area, is 5.2 ± 0.3 nm. This value is in a good agreement with the value found by the ex situ nanoshaving (4.7 ± 0.3 nm for 1000 ppm solution). Doughnut structures observed in the nanoshaved region have the height of ~10–15 nm and may be attributed to nanobubbles present on a water-covered HOPG surface[39].

Besides HOPG, the BSA films were also scrutinized on the mica-supported Au(111) surface, both by ex situ and in situ AFM imaging and nanoshaving techniques. The BSA film on monocrystalline gold was prepared from the 1000 ppm BSA solution. Figure 6 shows a typical ex situ 1 μm TM AFM image of the BSA film on Au(111) surface before (panel a) and after (panel b) CM AFM nanoshaving with the image size 0.3 μm.

Similarly to the BSA films formed on the HOPG substrate, holes may be observed in the film on Au(111), indicating the presence of the nanobubbles during the BSA adsorption[27,28]. Some spherical particles may be no-

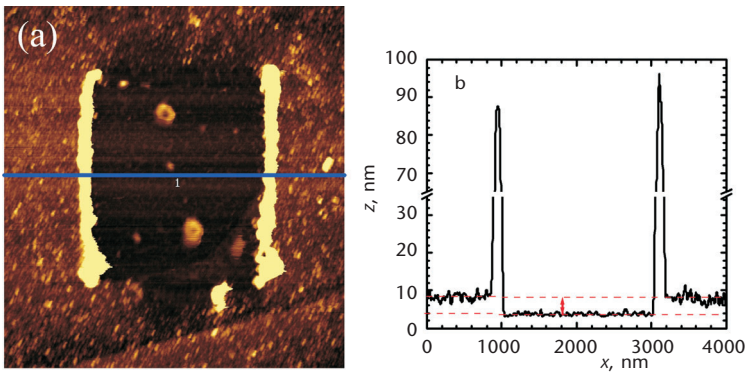

FIG. 5
Panel a shows the in situ TM AFM obtained after 2 × 2 μm nanoshaving. Image size 4 × 4 μm, height scale 15 nm. Typical profile is shown in the panel b. The dashed red lines denote the film thickness. The profile in panel b is obtained at the surface location corresponding to the solid blue line in panel a

ticed inside the holes, probably as a result of the BSA adsorption during the substrate water rinsing when the nanobubbles are destroyed. The nanoshaving procedure leads to the film thickness 2.3 ± 0.2 nm. This value was obtained as the average of thirty topography differences measured along the edges of two individual nanoshaved areas. The procedure was the same as that shown in Fig. 2. The average film thickness is identical to the average of the hole depth values, indicating that the hole bottom coincides with the Au(111) surface. The obtained film thickness is in a reasonable agreement with the value found by Tencer et al.[38] employing the ex situ nanoshaving (2 nm). In their work, the polycrystalline gold stripes were employed instead of the Au(111) surface. The value 2 nm was determined as a mean lowering of the nanoshaved area with respect to the neighboring pristine one. Here, we employ a more sophisticated approach based on the section analysis along the edges of the nanoshaved area. Moreover, we employ the monocrystalline Au surface.

On gold surfaces, the nanoshaving was accomplished with the constant repulsive force 34 nN. The same and even higher force values (tested up to 200 nN) did not lead to the damage of the underlying Au(111) surface (the corresponding images are not shown).

The BSA film on Au(111) surface was also investigated by in situ AFM imaging and nanoshaving in water. Figure 7 shows a typical in situ TM AFM image of BSA film on Au(111) in water before (panel a) and after (panel b) the CM AFM nanoshaving with the image size of 0.2 μm. Note that some material was partly re-adsorbed in the middle of the nanoshaved region

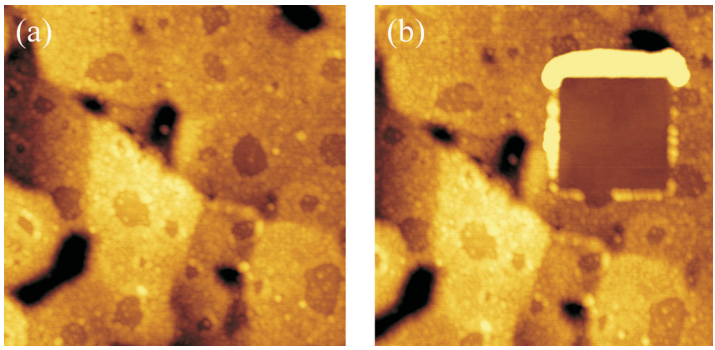

FIG. 6
BSA film on Au(111) surface imaged by ex situ TM AFM before (panel a) and after (panel b) nanoshaving with the image size 0.3 × 0.3 μm in the upper right part of the original image. Image size 1 × 1 μm, height scale 15 nm

(panel b). It happened possibly due to the diffusion of the BSA molecules back to the nanoshaved surface. Figure 7c shows the profiles before (solid red line) and after (dashed green line) the nanoshaving. The two profiles are obtained at the same location on the surface and are denoted by solid blue lines in panels a and b. Panel d shows the phase image of the area shown in panel b.

The in situ nanoshaving was performed at several sample locations, giving the average value of the film thickness 2.0 ± 0.2 nm, which well corresponds to the value found by us employing the ex situ technique (2.3 ± 0.2 nm). The value is identical to that found by Tencer et al.[38] employing the ex situ technique. Unlike the ex situ images, the film thickness found

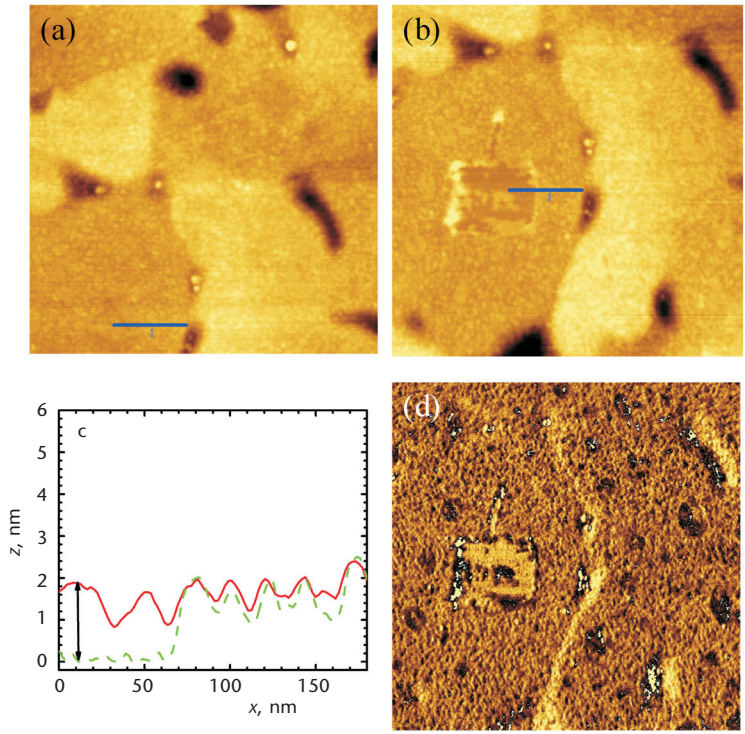

FIG. 7
In situ TM AFM images of BSA film on Au(111) before (panel a) and after (panel b) the nanoshaving (0.2 μm). The images are vertically shifted by ca. 400 nm. Panel c shows the profiles before (solid red line) and after (dashed green line) the nanoshaving. Profiles are obtained at the same location (solid blue lines in panels a and b). Panel d shows the phase image of the area in panel b. Image size 1 × 1 μm, height scale 17 nm

by the nanoshaving cannot be compared to the depth of the holes as they are missing in the in situ images. Instead, patch-like structures are well discernible in the phase image (see Fig. 7d). Phase imaging reveals the differences in the probe kinetic energy dissipation due to the interaction between the probe and the surface structures. The patch-like structures have the phase shift different from that observed on BSA-covered and nanoshaved regions. We suggest that the structures correspond to the holes observed in the-ex situ images (Fig. 6).

To summarize our results, the comparison of the film thickness values on Au(111) and HOPG determined by in situ and ex situ nanoshaving is shown in Table I.

TABLE I
Data are obtained by nanoshaving of the films formed from the solutions containing 1000 ppm BSA during the protein adsorption

Substrate	Ex situ thickness, nm	In situ thickness, nm
HOPG	4.7 ± 0.3	5.2 ± 0.3
Au(III)	2.3 ± 0.2	2.0 ± 0.2

For both surfaces, the thickness values obtained in situ and ex situ are in a good mutual agreement. Moreover, the values obtained on the Au(111) surface are in the accordance with those found by Tencer et al.[38]. The films formed on Au(111) are thinner than those on HOPG, due to a higher extend of the BSA denaturation on Au(111) surface. We conclude that both in situ and ex situ nanoshaving techniques are suitable for the analysis of protein films on monocrystalline surfaces and interfaces. The results presented here will be further utilized in the in-situ investigations focusing on the interactions between nanobubbles and nanopancakes and the BSA molecules.

This research was supported by the Czech Science Foundation (203/09/P502 and 203/08/1157).

REFERENCES

1. Šustrová B., Štulík K., Mareček V., Janda P.: *Electroanalysis* **2010**, *22*, 2051.
2. Fadrná R.: *Anal. Lett.* **2005**, *37*, 3251.
3. Liu G., Xu S., Qian Y.: *Acc. Chem. Res.* **2000**, *33*, 457.
4. Pişkin E.: *Hacettepe J. Biol. Chem.* **2007**, 35, 157.
5. Mendes P. M., Yeung C. L., Preece J. A.: *Nanoscale Res. Lett.* **2007**, *2*, 373.
6. Rosa L. G., Liang J.: *J. Phys.: Condens. Matter* **2009**, *21*, 483001.

7. Wendel M., Kuhn S., Lorenz H., Kotthaus J. P., Holland M.: *Appl. Phys. Lett.* **1994**, *65*, 1775.
8. Xu S., Liu G.: *Langmuir* **1997**, *13*, 127.
9. Xu S., Miller S., Laibinis P. E., Liu G.: *Langmuir* **1999**, *15*, 7244.
10. Piner R. D., Zhu J., Xu F., Hong S., Mirkin C. A.: *Science* **1999**, *283*, 661.
11. Sugimura H., Hanji T., Hayashi K., Tahai O.: *Adv. Mater.* **2002**, *14*, 524.
12. Simic-Milosevic V., Heyde M., Nilius N., Nowicki M., Rust H.-P., Freund H.-J.: *Phys. Rev. B* **2007**, *75*, 195416.
13. Ross C. B., Sun L., Crooks R. M.: *Langmuir* **1993**, *9*, 632.
15. Rezek B., Ukraintsev E., Michalíková L., Kromka A., Zemek J., Kobalcova M.: *Diam. Relat. Mater.* **2009**, *18*, 918.
16. Rezek B., Shin D., Nebel C. E.: *Langmuir* **2007**, *23*, 7626.
17. Varotto A., Todaro L., Vinodu M., Koehne J., Liu G., Drain C.: *Chem. Commun.* **2008**, 4921.
18. Brower T. L., Garno J. C., Ulman A., Liu G., Yan C., Gölzhäuser A., Grunze M.: *Langmuir* **2002**, *18*, 6207.
19. Kerstan A., Ladnorg T., Grunwald C., Vöpel T., Zacher D., Herrmann C., Wöll C: *Biointerphases* **2010**, *5*, 131.
20. Chwang A. B., Granstrom E. L., Frisbie C. D.: *Adv. Mater.* **2000**, *12*, 285.
21. Seo K., Borguet E.: *Langmuir* **2006**, *22*, 1388.
22. Staii C., Viesselmann C., Ballweg J., Shi L., Liu G., Williams J. C., Dent E. W., Coppersmith S. N., Eriksson M. A.: *Biomaterials* **2009**, *30*, 3397.
23. Lee M. V., Nelson K. A., Hutchins L., Becerril H. A., Cosby S. T., Blood J. C., Wheeler D. R., Davis R. C., Woolley A. T., Harb J. N., Linford M. R.: *Chem. Mater.* **2007**, *19*, 5052.
24. Wright A. K., Thompson M. R.: *Biophys. J.* **1975**, *15*, 137.
25. Peters T., Putman F. W. (Eds): *The Plasma Proteins*, p. 133. Academic Press, New York 1975.
26. Paleček E., Heyrovský M., Janík B., Kaláb D., Pechan Z.: *Collect. Czech. Chem. Commun.* **2009**, *74*, 1739.
27. Wu Z., Zhang X., Zhang X., Sun J., Dong Y., Hu J.: *Chin. Sci. Bull.* **2007**, *52*, 1913.
28. Wu Z., Chen H., Dong Y., Mao H., Sun J., Chen S., Craig V. S. J., Hu J.: *J. Colloid Interface Sci.* **2008**, *328*, 10.
29. Grybos J., Marszalek M., Lekka M., Heinrich F., Tröger W.: *Hyperfine Interact.* **2004**, *159*, 323.
30. Mori O., Imae T.: *Colloids Surf., B* **1997**, *9*, 31.
31. Lai C., Motta N., Bell J. M.: *Int. J. Nanosci.* **2008**, *7*, 299.
32. Ta T. C., McDermott M. T.: *Colloids Surf., B* **2003**, *32*, 191.
33. Stobiecka M., Hepel M., Radecki J.: *Electrochim. Acta* **2005**, *50*, 4873.
34. Yu Y., Ying P. Q., Jin G.: *Chin. Chem. Lett.* **2004**, *15*, 1465.
35. Ohtsuka I., Yokoyama S.: *Chem. Pharm. Bull.* **2005**, *53*, 42.
36. Valle-Delgado J. J., Molina-Bolívar J. A., Galisteo-González F., Gálvez-Ruiz M. J., Feiler A., Rutland M. W.: *J. Phys. Chem. B* **2004**, *108*, 5365.
37. Shi J., Chen J., Cremer P. S.: *J. Am. Chem. Soc.* **2008**, *130*, 2718.
38. Tencer M., Charbonneau R., Lahoud N., Berini P.: *Appl. Surf. Sci.* **2007**, *253*, 9209.
39. Janda P., Frank O., Bastl Z., Klementová M., Tarábková H., Kavan L.: *Nanotechnology* **2010**, *21*, 095707.